Salisbury, M.H., Shinohara, M., Richter, C., et al., 2002
Proceedings of the Ocean Drilling Program, Initial Reports Volume 195

6. Measurement of Hydraulic Conductivity and Specific Storage Using the Shipboard Manheim Squeezer[1]

D.J. Hart[2] and W.S. Hammon III[3]

INTRODUCTION

Measurement of hydraulic conductivity and specific storage of ocean-bottom sediments is important for understanding the flow patterns and residence times of the pore fluids found in those sediments. Often, those parameters are measured using both an oedometer to measure the consolidation coefficient and specific storage and a permeameter to measure the hydraulic conductivity. Although this combination gives the most accurate measurements, these two items are not part of the usual shipboard complement of apparatus. Furthermore, it may not be possible to conduct the measurements in both apparatus because of either a limited amount of sample or the space limitations for laboratory equipment on board the ship. The Manheim squeezer, designed to extract pore fluids from unconsolidated material, is part of the usual shipboard apparatus. During Leg 195, the Manheim squeezer was used to conduct consolidation tests, which resulted in estimations of the hydraulic conductivity and specific storage of serpentine muds. These muds were recovered from the South Chamorro Seamount (Ocean Drilling Program [ODP] Site 1200), drilled in the Mariana forearc (Fig. **F1**) during ODP Leg 195. The methodology, assumptions, and results from these tests are presented below.

F1. Location of the South Chamorro serpentine mud volcano, p. 10.

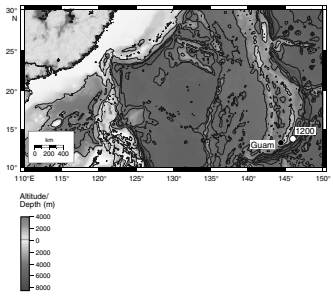

[1]**Examples of how to reference the whole or part of this volume.**

[2]Wisconsin Geological and Natural History Survey, University of Wisconsin-Extension, Madison WI 53705-5100, USA.
djhart@facstaff.wisc.edu
[3]Center for Lithospheric Studies, University of Texas at Dallas, PO Box 830688, Richardson TX 75083-0688, USA.

Ms 195IR-106

TEST METHOD

Overview of Test

In this test, as in many consolidation tests (Taylor, 1948), a constant axial load applied using an external loading frame was instantaneously applied to a sample of unconsolidated material that was laterally constrained. The axial load produced an excess pore fluid pressure along the length of the sample, except at the bottom of the sample. The bottom of the sample was drained so that there was no excess pore fluid pressure; the pressure at the bottom of the sample was atmospheric. Fluid flowed from the sample bottom because of this pressure gradient, and the total amount of fluid discharged was measured as a function of time. Figure F2A is a diagram of the apparatus and the assumed boundary conditions. Figure F2B is an idealized pressure profile along the length of the sample with increasing time. This test differed from the usual consolidation test in that the process was not repeated for larger axial stresses after the pore pressure dissipated. We were most interested in the hydraulic conductivity and specific storage, not the past stress history of the samples.

F2. Experimental apparatus with boundary conditions and pore pressure profiles, p. 11.

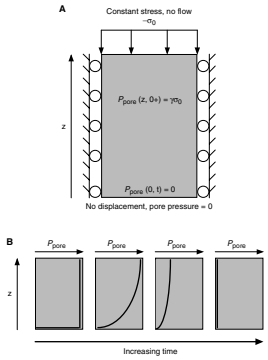

Sample Preparation

Immediately after the core was recovered, a 6-in length of whole-round core was cut and stored under refrigeration until testing. Samples for testing from these cores were removed from the whole-round core using a piston core sampler with the same diameter as the Manheim squeezer (diameter = 4.25 cm). The initial lengths of the samples were ~3 cm. In most cases, two samples were tested from each whole round, one sample oriented with its axis parallel to vertical and one with its axis perpendicular to vertical. The samples were loaded individually into the Manheim squeezer, which was then placed in the load frame and loaded to a predetermined axial stress.

Test Description

Figure F3 is a diagram of the Manheim squeezer. After the core was loaded into the Manheim squeezer, the axial load was applied using a hydraulic ram in a loading frame. The axial loads were held relatively constant (±10%) by watching and adjusting the load as needed over the course of a test. The axial loads were measured using a mechanical gauge on the hydraulic ram. These loads were greater than those commonly used in consolidation tests because of the limited dial resolution and accuracy of the gauge on the hydraulic ram. The lowest possible accurate reading of the gauge (2000 lb) corresponded to an axial stress of 6.3 MPa on the sample. This corresponds to a burial depth of ~230 m, if the contribution to effective stress from pore pressure is neglected.

F3. Diagram of the Manheim squeezer, p. 12.

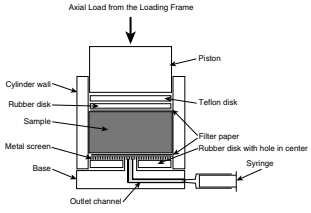

The fluid discharge as a function of time was measured using a 10-mL syringe and a stopwatch. The assumption of incompressible mineral grains and water, common to soil mechanics (Wang, 2000), allowed the volume of water displaced from the sample to be converted to axial displacement using the cross-sectional area of the cylinder,

$$\Delta w = \text{volume of water discharged/cross-sectional area of cylinder,} \quad (1)$$

where Δw = axial displacement.

Although this method is experimentally simple, it may introduce errors in measurement due to frictional effects between the syringe plunger and cylinder. If >10 mL of fluid was discharged, the full syringe was quickly replaced with an empty 10-mL syringe. The time needed for 10 mL of discharge was generally greater than an hour, so the discharge rate was low and no fluid was lost. A test was generally run for several hours, with the operator holding the axial load constant and recording data until there was no more discharge from the sample.

DATA ANALYSIS

These data were analyzed to determine estimates of hydraulic conductivity and specific storage using two different methods, the square root of time method and a variable-thickness deformable-element finite difference routine. Estimates of hydraulic conductivity and specific storage were found by fitting curves produced by these models to the data. Figure F4 shows data from one of the runs on Sample 195-1200E-5H-3, 51–61 cm, and curve fits of the two methods of analysis, square root of time (Fig. F4A) and finite difference (Fig. F4B). The square root of time method is quickly and easily applied but involves more assumptions, whereas the finite difference method, although more cumbersome, removes some assumptions.

F4. Comparison between the two test methods, p. 13.

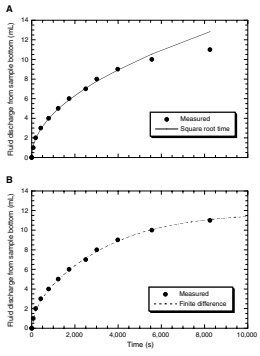

Square Root of Time Method

To analyze the data using the square root of time method, we use the relationship for displacement in a semi-infinite length cylinder as a function of time (Terzaghi, 1943; Taylor, 1948; Wang, 2000), as follows:

$$\Delta w(t) = 2c_m\gamma\sigma_z \times \mathrm{SQR}(Dt/\pi), \quad (2)$$

where,

c_m = the vertical compressibility,
γ = the loading efficiency,
σ_z = the axial load, and
D = the hydraulic diffusivity.

We can determine the lumped product of constants on the right hand side of Equation 3 by calculating the slope of the displacement vs. the square root of time, as follows:

$$\Delta w/\mathrm{SQR}(t) = 2c_m\gamma\sigma_z \times \mathrm{SQR}(D/\pi). \quad (3)$$

Only the early time portion of the plot, from 0 to 2500 s, is used to determine the slope (Fig. F4). The rest of the data points from 3000 to 9000 s are neglected. At early times, the pore pressure decrease has not yet diffused to the end of the sample (see Fig. F2) and so the approximation of a semi-infinite cylinder is still valid. To determine the hydraulic diffusivity (D) from the lumped product in Equation 3, we need to determine the other unknown factors of the lumped product, c_m and γ.

The vertical compressibility is defined by the following equation:

$$c_m = (\Delta w/w_0)/\Delta\sigma_z|_{e_{rr}=0,\ \Delta P_{pore}=0}. \quad (4)$$

Because all the components of Equation 4 (axial displacement [Δw], axial stress [σ_z], and sample length [w_0]) were measured, it is possible to calculate the vertical compressibility. Also, the conditions of no radial strain ($e_{rr} = 0$) and no change in pore pressure ($\Delta P_{pore} = 0$) were valid because the stiff cylinder wall prevented radial strain and the pore pressure throughout the entire length of the sample returns to atmospheric pressure at very long times. However, the assumption of infinitesimal strain is not well met in these measurements. The estimated strain for the sample whose data are shown in Figure F4 is ~20%, a typical value for these tests.

The loading efficiency is defined as the following:

$$\gamma = \Delta P_{pore}/\Delta\sigma_z|_{e_{rr}=0}, \quad (5)$$

where P_{pore} = the pore fluid pressure. The assumption of incompressible grains and pore fluid lead to a value for γ of 1 (Wang, 2000). Given that c_m and γ have been determined, the hydraulic diffusivity (D) can be calculated using Equation 3.

Assuming the grains and pore fluid are incompressible, the specific storage (S_s) can be calculated by the following equation:

$$S_s = c_m \times \rho_f \times g, \quad (6)$$

where,

ρ_f = the fluid density and
g = the acceleration of gravity.

Finally, we can determine the hydraulic conductivity (K) from the hydraulic diffusivity and specific storage using Equation 7:

$$K = D \times S_s. \quad (7)$$

This method suffers from having to make the assumption of a semi-infinite cylinder and then making the decision of how much of the data to include when calculating the slope to estimate the lumped product of constants in Equation 3. In Figure F4, we chose to include only those data recorded from 0 to 2500 s, but that decision was subjective. The second method of data analysis, finite difference, does not assume a semi-infinite cylinder, nor does it assume that the strains are infinitesimal. The sample deforms in response to the amount of fluid that has been discharged.

Deformable-Element Finite Difference Method

The finite difference method removes the need for assuming a semi-infinite cylinder and incorporates the shortening of the sample (finite strains) as pore fluid drains from the sample bottom. Like the square root of time method, it assumes that the grains and pore fluid are incompressible so that $\gamma = 1$ and Equation 6 is valid. Inputs for this routine are initial guesses for the hydraulic conductivity and the specific storage and measured values for the final sample length, the applied axial load, and the area of the cylinder. Using Equations 4, 5, and 6 and

the specific storage estimate supplied by the user, the initial length of the sample is calculated. It is this calculation that will ultimately constrain the value of the specific storage. Using this initial length, the sample is divided into 25 elements by the finite difference routine. Initial head values are input by setting the head at the sample bottom equal to zero and by setting the heads throughout the rest of the model equal to values calculated using Equation 5 and the applied axial load, as follows:

$$h_{initial} = \Delta P_{pore}/(\rho_f \times g) = \gamma \Delta \sigma_z/(\rho_f \times g). \quad (8)$$

To calculate the heads at subsequent time steps, the explicit finite difference approximation was used, although the Crank-Nicolson approximation (Wang and Anderson, 1982) might also have been employed. Following each time step, the length of each element was recalculated using the following definition of storativity (specific storage multiplied by element length) and the assumptions of incompressible grains and pore fluid:

$$\Delta(\Delta x_i) = S_s(h^n{}_i - h^{n+1}{}_i)\Delta x_i, \quad (9)$$

where,

Δx_i = the length of element *i,*
$\Delta(\Delta x_i)$ = the change in length of element *i,* and
$(h^n{}_i - h^{n+1}{}_i)$ = the change in head between time steps *n* and *n* + 1 at element *i.*

These new model lengths were then used in the next time step to calculate the heads at the next time step.

The outflow at the sample bottom (Q_n) was also calculated at each time step (n) using the following equation:

$$Q_n = -\text{area} \times K(\Delta h^n{}_1/\Delta x_1), \quad (10)$$

where Δh_1 and Δx_1 are the head and element thickness, respectively, of the bottom element. The heads at the nodes and the outflow at the sample bottom for each time step were recorded as the model stepped through time. When the model reached the end time, set to be after the last recorded data point for the sample, the model results for the outflow and data of outflow were plotted on the same graph and compared. The initial guesses of the hydraulic conductivity and specific storage were then varied to improve the fit and the model was rerun until a satisfactory fit between the model and the recorded data was found. A formal inversion could be implemented to better fit the data and give sensitivities of the hydraulic conductivity and specific storage to the data.

A check was performed to ascertain that the cumulative discharge ($\Sigma_N Q_n$), determined by summing the discharges calculated in Equation 10, was still equal to displacement, calculated by summing the length of all the elements at time step n, multiplied by the area. The two results agreed to better than 0.1% difference.

DISCUSSION OF RESULTS AND ASSUMPTIONS

The results of these tests on 12 serpentine mud samples are shown in Table T1, along with the corresponding depths and porosities. For comparison, the results of both methods of analysis, the square root of time model and the finite difference model, are presented. In general, the two methods give similar results, with the values of hydraulic conductivity estimated using the finite difference code being on average ~20% less than the values estimated using the square root of time analysis. There is less difference, on average, between the estimates of specific storage using the two methods.

T1. Results of consolidation tests, p. 15.

Repeatability of the measurements was checked on two of the cores, Samples 195-1200D-1H-3, 120–130 cm, and 1H-5, 10–20 cm. Two cores were taken from both of these samples and tests were run on them (Table T1). In both tests, the difference between the two measurements was ~20% when using the results from the finite difference method and ~30% when using the square root of time method. Although a sample size of only two is too small to generalize, this result suggests that the finite difference method does a slightly better job of estimating the flow parameters.

Figure F5A shows hydraulic conductivity as a function of depth. At shallow depths (<5 m), the values are ~10–20 × 10^{-11} m/s and then decrease rapidly with depth to nearly constant values of ~4 × 10^{-11} m/s below a depth of 20 mbsf. The specific storage behaves in a similar manner, except that it decreases only by a factor of about one-half instead of by one-fourth as the depth increases. Porosity vs. depth for all the serpentine muds samples measured during Leg 195 (Fig. F5B) shows a similar trend of decreasing values with depth. The porosity values given in Table T1 are from samples located within depths of 1 m from the samples used for the hydraulic conductivity measurements, and so the variability of those measurements may mask the general trend shown in Figure F5B.

F5. Hydraulic conductivity and porosity, Holes 1200D and 1200E, p. 14.

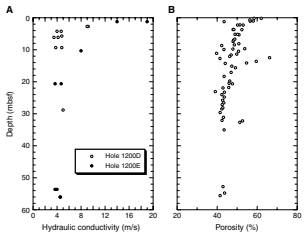

The dependence of the hydraulic conductivity and the specific storage on the axial load used during the test was also investigated. As can be seen in Table T1 for Sample 195-1200D-1H-4, 120–130 cm, a larger axial load resulted in decreased values of both the hydraulic conductivity and the specific storage. The larger load results in greater consolidation so that the flow paths through the material are restricted. This consolidation would also reduce the porosity so that the storage is also reduced. The hydraulic conductivity decreased more than the specific storage so that the hydraulic diffusivity, the ratio of the hydraulic conductivity to the specific storage, experienced a net decrease.

The average ratio of anisotropy (vertical/horizontal) of hydraulic conductivity was found to be 0.82 for the seven samples from which both horizontal and vertical cores were taken and tested. This anisotropy may be due to grain fabric aligned with the horizontal plane. This observation might warrant further investigation.

Several of the assumptions made in the above analysis may not be well met when using the Manheim squeezer. Chief among these is the assumption that there is no friction between the cylinder walls and both the piston and the sample sides as the sample is consolidated. This assumption would result in an underestimation of the vertical compressibility because the applied load used in the calculation would actually be reduced by friction. Using Equations 6 and 7, we can see that an

underestimation of the vertical compressibility would result in underestimation of the specific storage and the hydraulic conductivity.

We assumed that the pore fluid pressure is atmospheric at the sample bottom as fluid moves into the syringe. It may be that the syringe produced some backpressure due to friction between the syringe plunger and the syringe wall. This backpressure could be measured to determine if it is significant relative to the pore pressure in the sample during the test. Although it would add to the complexity of the testing apparatus, use of displacement transducers to measure the axial displacement would remove the need for using fluid discharge as a proxy for axial displacement.

We attempted to determine whether the volume of the outlet channel might decrease the initial discharge rate; the outlet channel would need to fill before any fluid could be measured in the syringe. We did several runs with the outlet channel filled with deionized water and did not note any significant difference between runs where we did not fill the channel. It may be that the air in the channel was displaced into the syringe, and so if the friction between the syringe wall and piston was low, the air would displace the piston as easily as the water and there would be little error introduced. Even if the air did not displace the syringe piston, the volume of the outlet channel was ~0.5 mL and so would affect the total fluid discharged by only ~5%.

Another assumption is that the sample was fully saturated. We know this was not the case, as some gas bubbles (~1 mL, or 5%–10% of the total discharged volume) were discharged into the syringe during most of the tests. This gas came out of solution when the sample was brought from the ocean bottom to the surface. The sample should be resaturated so that this gas would not be present. The presence of gas would affect the results by increasing the vertical compressibility of the sample by introducing a highly compressible pore fluid, thus increasing the specific storage, and by introducing two-phase flow, reducing the hydraulic conductivity.

Last, we assumed that the hydraulic conductivity and the specific storage do not depend on the degree of consolidation. This assumption is common to all estimations of hydraulic conductivity and specific storage when using a consolidation test. That this assumption is not true is apparent in all the fits of the finite difference model to the measured data. At early times, up to 1000 s in Figure **F4B,** the finite difference model underestimates the fluid discharge and then later, after 5000 s, overestimates the fluid discharge. This pattern is common to all the finite difference model fits and cannot be removed by variation of the parameters without gross misfit to the data. This pattern can be explained if the hydraulic diffusivity decreases with consolidation. Less of the material is consolidated at early times and so fluid flows more quickly. Our measurements of hydraulic conductivity and specific storage for these samples represent weighted average values obtained over a very wide range of consolidation states. For Sample 195-1200E-5H-3, 51–61 cm, shown in Figure **F4,** the porosity of the sample decreased from 48% at the start of the test to 28% at the end of the test. It should be noted that this dependence is not apparent using the square root of time method of analysis.

CONCLUSIONS

The Manheim squeezer can be used to measure hydraulic conductivity and specific storage. As determined by these tests, the serpentine muds of the South Chamorro Seamount have hydraulic conductivities ranging from 1.0×10^{-11} to 1.9×10^{-10} m/s and specific storages ranging from 3×10^{-5} to 6.3×10^{-4} m^{-1}. These values can be used to constrain consolidation times and fluid flow patterns in the serpentine mud seamounts of the Mariana forearc. However, further testing should be done to determine how well this apparatus meets the boundary conditions of consolidation tests. The analysis showed that the hydraulic conductivity and specific storage depend on the degree of consolidation and the applied axial load. Although the square root of time method and the finite difference method give similar results, the finite difference method might allow investigation of nonlinear behavior of the hydraulic conductivity and specific storage that would otherwise not be apparent using only the square root of time method.

ACKNOWLEDGMENTS

This research used samples and/or data provided by the Ocean Drilling Program (ODP). ODP is sponsored by the U.S. National Science Foundation (NSF) and participating countries under the management of Joint Oceanographic Institutions (JOI), Inc. Funding for this research was provided by ODP award USSSP 195-F001314, and the data were obtained during ODP Leg 195.

REFERENCES

Taylor, D.W., 1948. *Fundamentals of Soil Mechanics:* New York (Wiley).
Terzaghi, K., 1943. *Theoretical Soil Mechanics:* New York (Wiley).
Wang, H.F., 2000. *Theory of Linear Poroelasticity with Applications to Geomechanics and Hydrogeology:* Princeton, N.J. (Princeton Univ. Press).
Wang, H.F., and Anderson, M.P., 1982. *Introduction to Groundwater Modeling:* New York (W.H. Freeman Co.).

Figure F1. Location of the South Chamorro serpentine mud volcano (ODP Site 1200).

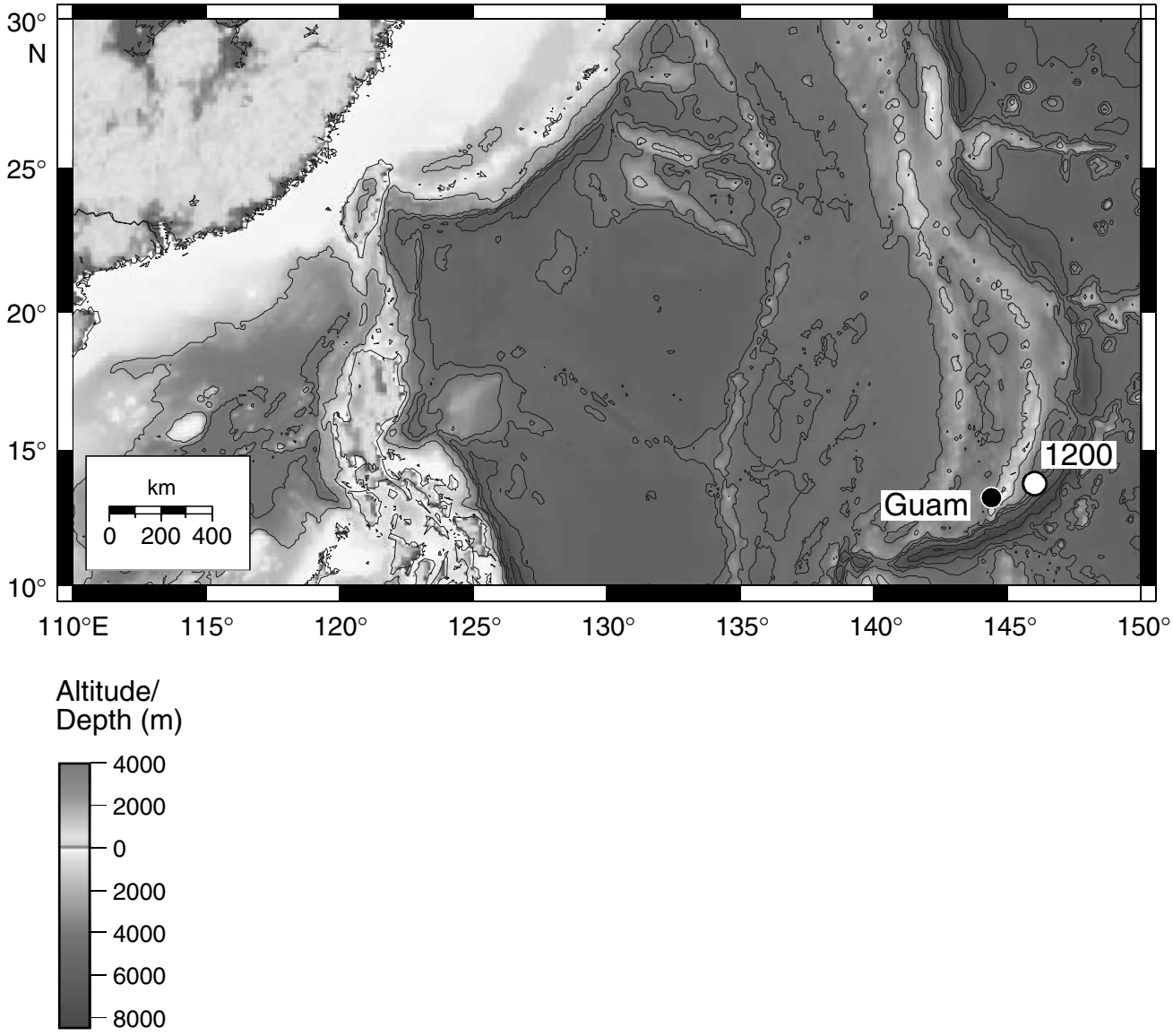

Figure F2. (**A**) Drawing of the experimental apparatus with boundary conditions and (**B**) the pore pressure profiles with increasing time.

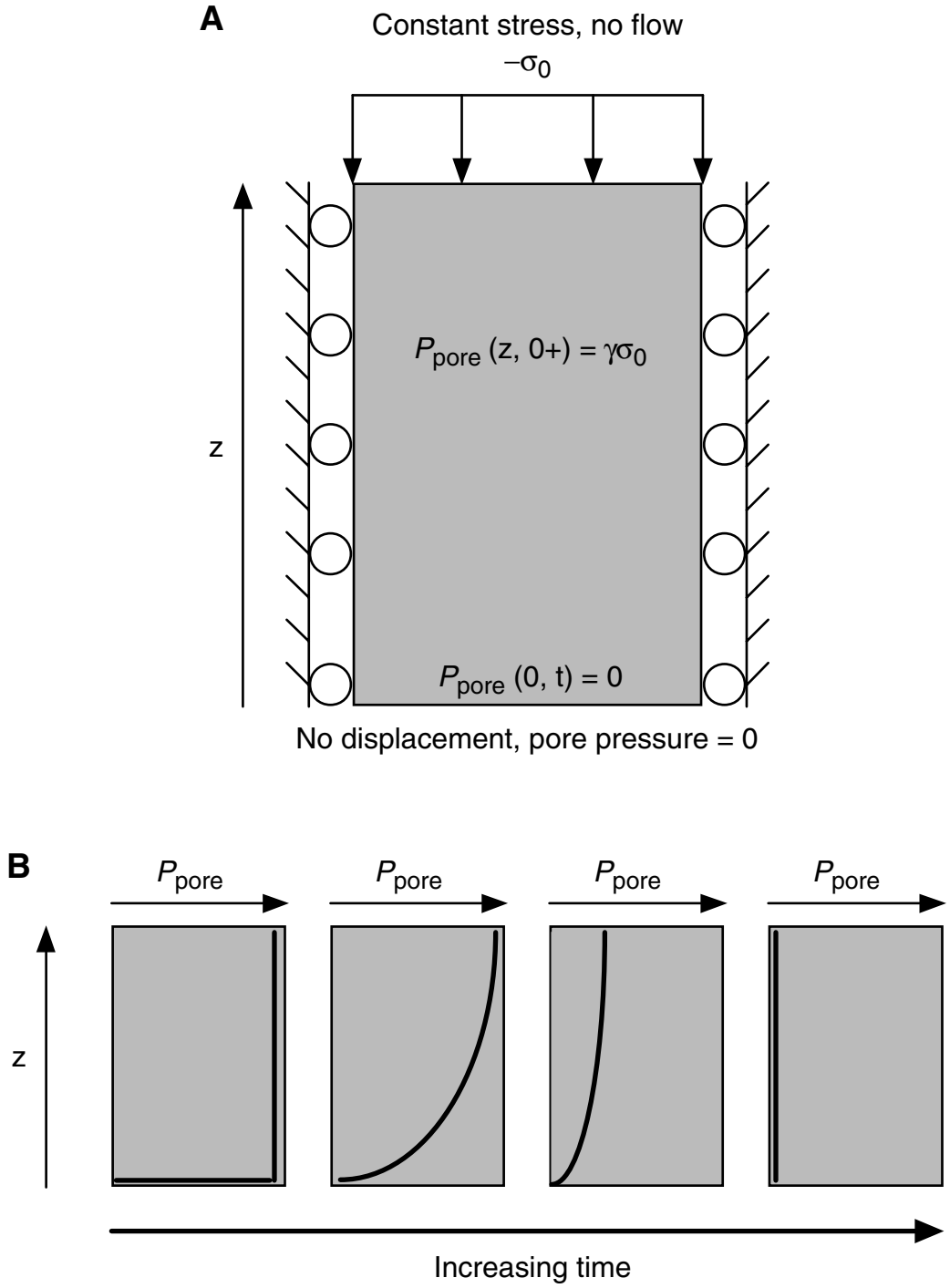

Figure F3. Diagram of the Manheim squeezer.

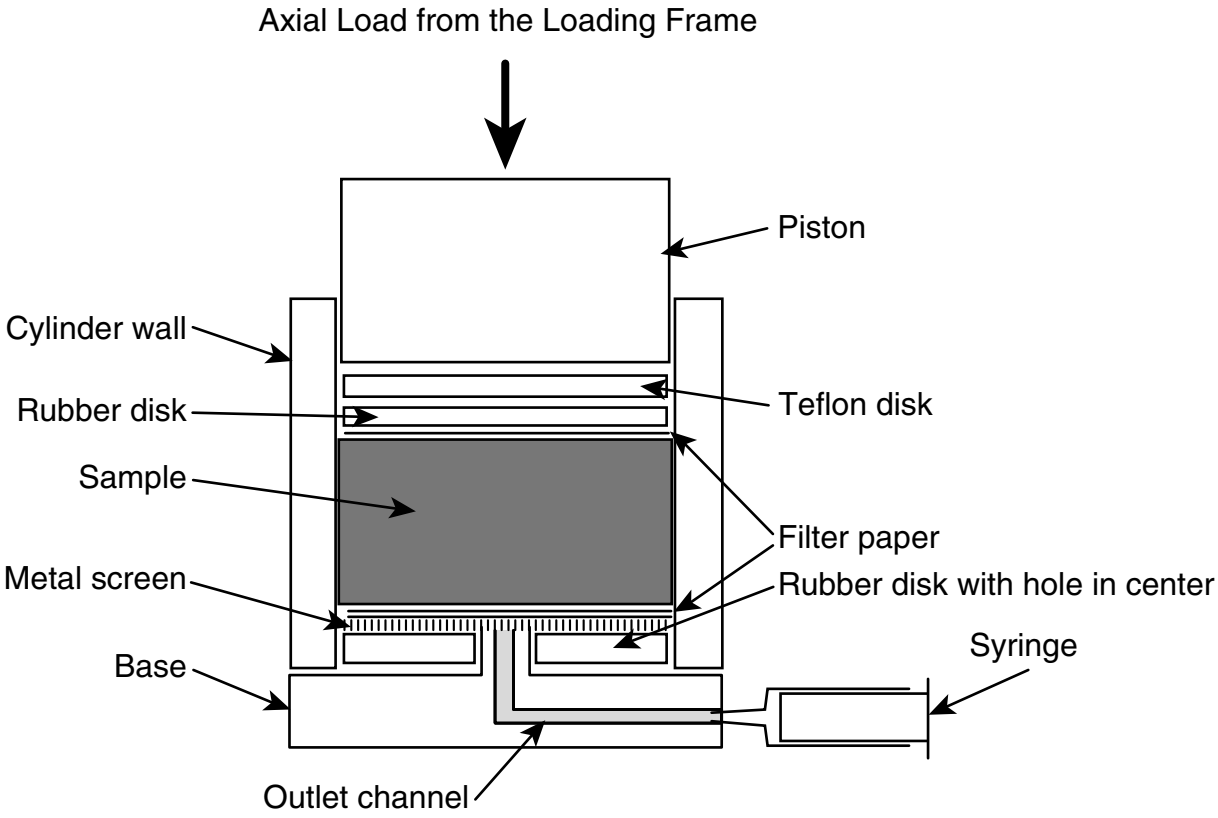

Figure F4. A. Comparison between the measured fluid discharge (circles), and the square root of time solution for a semi-infinite length sample (solid line) for Sample 195-1200E-5H-3, 51–61 cm. **B.** Comparison between the measured fluid discharge (circles) and the finite difference solution (dashed line) for Sample 195-1200E-5H-3, 51–61 cm. The fluid discharge is proportional to axial strain. Note that at longer times the measured discharge and the finite difference solution approach an asymptotic value of discharge, whereas the square root of time discharge will increase without bound.

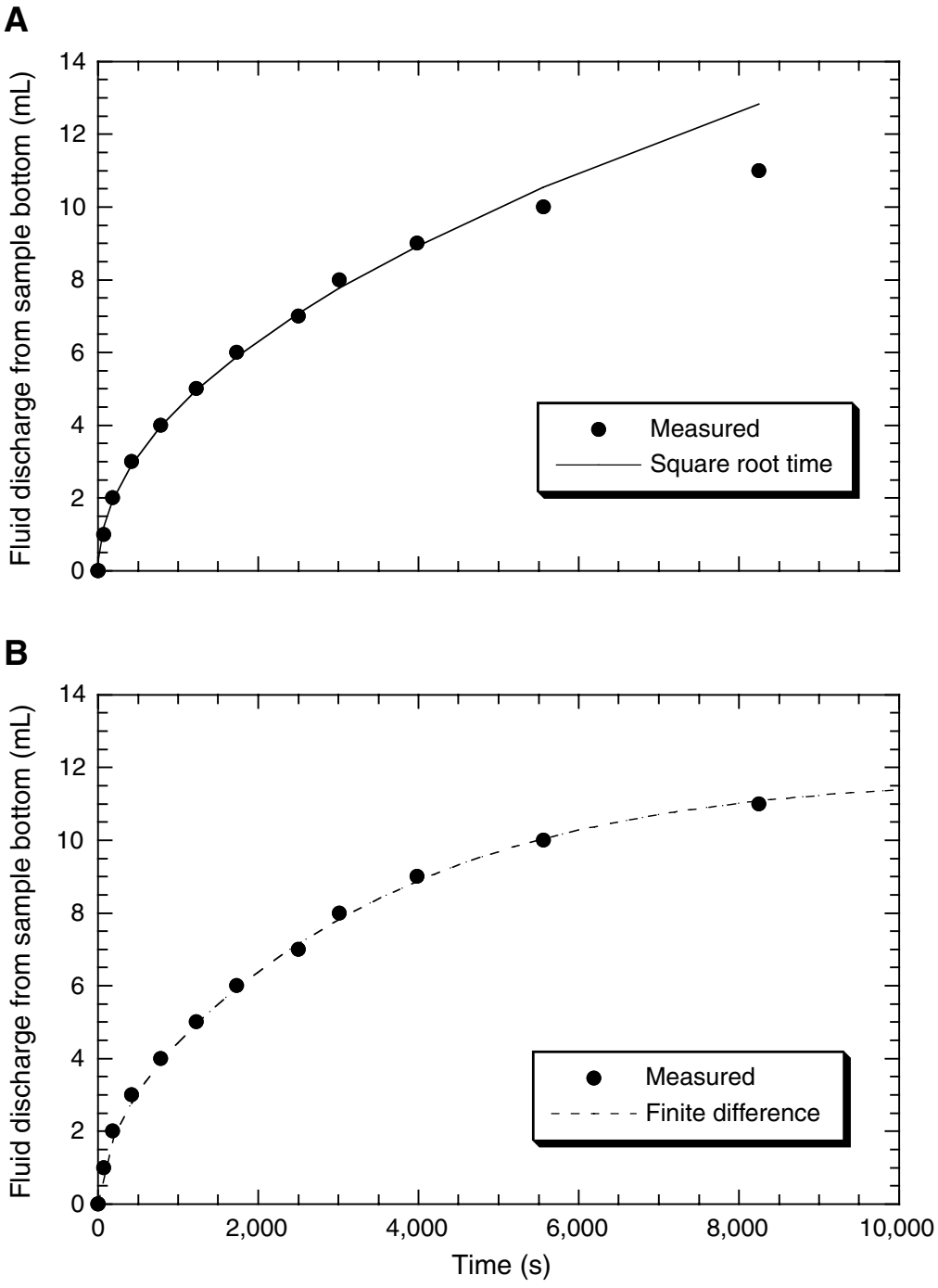

Figure F5. A. Hydraulic conductivity as a function of depth for Holes 1200D and 1200E. **B.** Porosity as a function of depth for Holes 1200D and 1200E. The curve of decreasing porosity with depth is similar to the curve of hydraulic conductivity with depth.

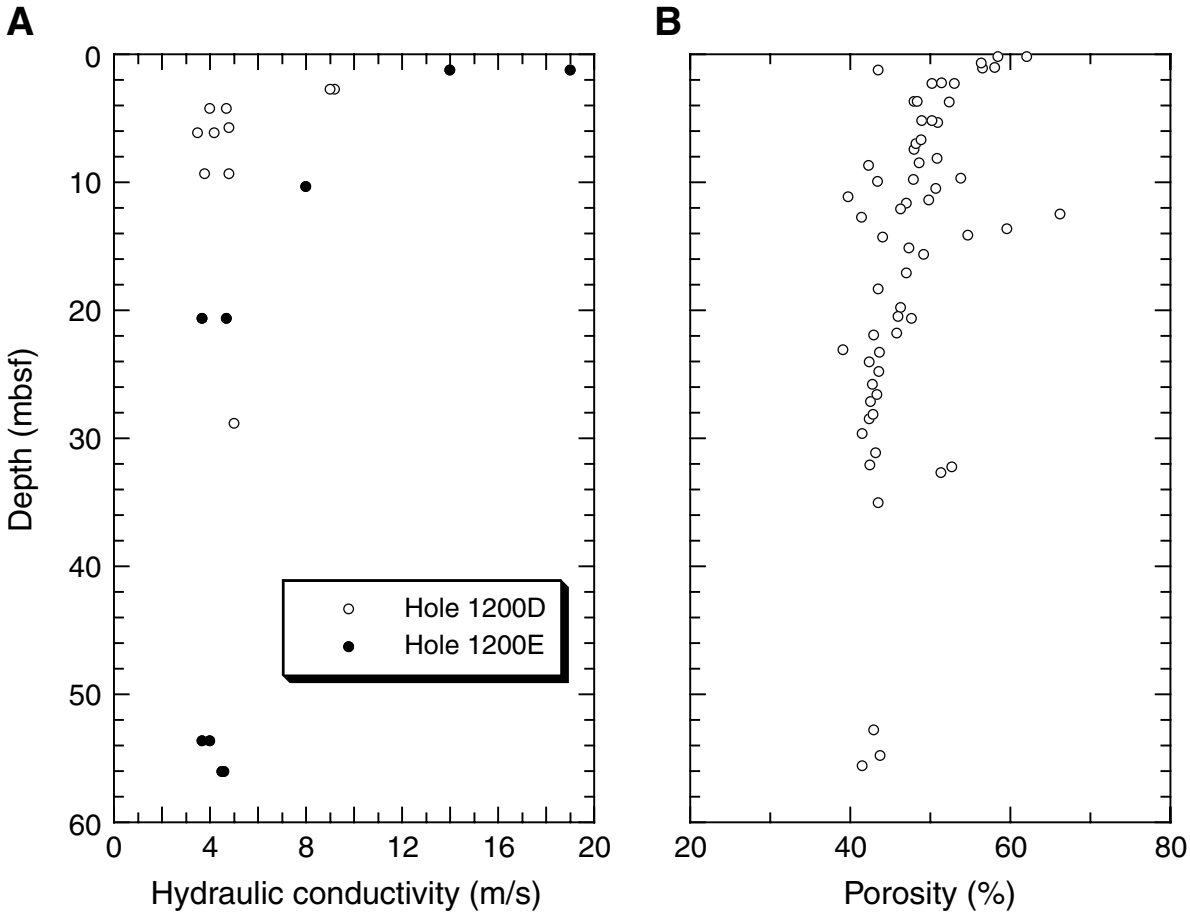

Table T1. Results of consolidation tests using the Manheim squeezer.

Core, section, interval (cm)	Depth (mbsf)	Square root time model		Finite difference model		Sample axis alignment	Axial load (MPa)	Porosity (%)
		Hydraulic conductivity (m/s) × 10^{-11}	Specific storage (m^{-1}) × 10^{-4}	Hydraulic conductivity (m/s) × 10^{-11}	Specific storage (m^{-1}) × 10^{-4}			
195-1200D-								
1H-2, 121–130	2.75	11.2	5.3	9.2	5.0	Vertical	6.3	44
		12.1	5.5	9.0	5.3	Horizontal	6.3	
1H-3, 120–130	4.25	4.4	3.4	4.0	3.4	Vertical	6.3	48
		5.7	4.4	4.7	4.3	Vertical	6.3	
1H-4, 120–130	5.75	1.7	0.7	3.0	0.3	Vertical	63.0	49
		5.6	3.8	4.8	3.8	Vertical	6.3	
1H-5, 10–20	6.15	3.9	3.5	3.5	3.5	Vertical	6.3	NA
		5.3	3.3	4.2	3.5	Vertical	6.3	
2H-2, 88–98	9.33	4.2	3.2	3.8	3.1	Vertical	6.3	52
		6.0	3.6	4.8	3.4	Horizontal	6.3	
9H-1, 80–90	28.85	5.2	3.4	5.0	3.0	Vertical	6.3	43
195-1200E-								
1H-1, 120–130	1.25	24.4	5.8	14.0	6.0	Vertical	6.3	58
		27.5	5.8	19.0	5.4	Horizontal	6.3	
2H-3, 123–133	10.38	9.0	3.2	8.0	3.2	Vertical	6.3	48
5H-3, 51–61	20.67	5.6	3.2	3.7	6.3	Vertical	6.3	48
		5.8	3.3	4.7	3.5	Horizontal	6.3	
7H-5, 30–40	32.25	1.1	0.6	1.0	0.6	Vertical	31.4	53
		1.4	1.2	1.9	0.8	Horizontal	31.4	
10H-1, 120–130	53.65	4.0	1.9	3.7	1.9	Vertical	6.3	43
		4.1	1.7	4.0	1.7	Horizontal	6.3	
10H-3, 62–72	56.07	4.4	2.5	4.5	2.2	Vertical	6.3	42
		4.4	2.5	4.6	2.1	Horizontal	6.3	

Note: NA = not available.